Available online at BCREC website: https://bcrec.id

Bulletin of Chemical Reaction Engineering & Catalysis, 17 (1) 2022, 88-102

Research Article

The Ni Catalyst Supported on the FSP-made Transition Metal (Co, Mn, Cu or Zn) Doped La_2O_3 Material for the Dry Reforming of Methane

Phakampai Aunmunkong, Choowong Chaisuk*

Department of Chemical Engineering, Faculty of Engineering and Industrial Technology, Silpakorn University, Nakhon Pathom 73000, Thailand.

Received: 15th October 2021; Revised: 21st November 2021; Accepted: 22nd November 2021
Available online: 24th November 2021; Published regularly: March 2022

Abstract

The transition metal (Co, Mn, Cu or Zn) doped La_2O_3 material was prepared by flame spray pyrolysis (FSP) technique. The 2 wt.% Ni catalyst supported on this material was characterized by XRD, N_2 physisorption, TPR, H_2 chemisorption and TGA, and evaluated by the dry reforming of methane (DRM). The perovskite structure was certainly formed when either Co or Mn was introduced. The Cu can generate the La_2CuO_4 spinel phase while the Zn showed a mixed phase of La_2O_3, ZnO and $La(OH)_3$. The Ni/Co-La_2O_3 catalyst was more active for the DRM because of high amount of active dual sites of Ni and Co metals dispersed on the catalyst surface. The formation of $La_2O_2CO_3$ during the reaction can inhibit the coke formation. The cooperation of $La_2O_2CO_3$ and MnO phases in the Ni/Mn-La_2O_3 catalyst was promotional effect to decrease carbon deposits on the catalyst surface. The partial substitution of Co for Mn with a small content of Mn can enhance the catalytic activity and the product yield. The Ni/$Mn_{0.05}Co_{0.95}$-La_2O_3 catalyst showed the highest CH_4 conversion, H_2 yield and H_2/CO ratio. The Mn inserted into the perovskite structure of $LaCoO_3$ was an important player to change oxygen mobility within the crystal lattice to maintain a high performance of the catalyst.

Keywords: Ni/Co-La_2O_3; Ni/Mn-La_2O_3 Flame spray pyrolysis; Perovskite; Dry reforming of methane

How to Cite: P. Aunmunkong, C. Chaisuk (2022). The Ni Catalyst Supported on the FSP-made Transition Metal (Co, Mn, Cu or Zn) Doped La_2O_3 Material for the Dry Reforming of Methane. *Bulletin of Chemical Reaction Engineering & Catalysis*, 17(1), 88-102 (doi:10.9767/bcrec.17.1.12501.88-102)

Permalink/DOI: https://doi.org/10.9767/bcrec.17.1.12501.88-102

1. Introduction

It is well-known that global warming is caused by emission of greenhouse gases including carbon dioxide carbon dioxide (CO_2), methane (CH_4), nitrous oxides (N_2O), chlorofluorocarbon (CFC) and ozone (O_3). The CO_2 and CH_4 have cause the global temperature to raise, polar ice to melt, loss of balance to the ecosystem and natural disasters [1–3]. The CO_2 reforming of CH_4 or the dry reforming of methane (DRM) reaction attracts interest for converting CO_2 and CH_4 to the syngas (CO and H_2). The DRM not only helps in decreasing toxic airborne emissions but also allows production of the syngas with a H_2/CO ratio equal to unity. This syngas is the starting feedstock of methanol synthesis and Fischer-Tropsch synthesis (FTS) [4]. The main reaction of the DRM is expressed in Equation (1). In general, this reaction is able of promoting other undesired reactions, which are the reverse water gas shift reaction, the methane decomposition, and the Boudouard's reaction as shown in the Equations (2)-(4), respectively [5,6]. The DRM is highly endothermic reaction

* Corresponding Author.
Email: chaisuk_c@su.ac.th (C. Chaisuk);
Telp: +66-81-4203022, Fax: +66-34-252459

and requires high temperatures to obtain high conversions of methane [7]. As a consequence, the major problem is catalyst deactivation due to the accumulation of carbon on the catalyst surface and sintering at high temperature [8,9].

$CH_4 + CO_2 \leftrightarrow 2CO + 2H_2$ $\Delta H = 247$ kJ.mol^{-1} (1)
$CO_2 + H_2 \leftrightarrow H_2O + CO$ $\Delta H = 41$ kJ.mol^{-1} (2)
$CH_4 \leftrightarrow 2H_2 + C$ $\Delta H = 75$ kJ.mol^{-1} (3)
$2CO \leftrightarrow CO_2 + C$ $\Delta H = -172$ kJ.mol^{-1} (4)

The Ni based catalyst is commonly used in the DRM due to its high activity, low cost and availability [10–12]. However, the deactivation caused by carbon deposition still occurs on this catalyst. Many published works have reported the development of Ni catalysts to maintain high activity and show high resistance to carbon [13–15]. These are dependent on many factors such as nickel dispersion, supports, promoters, conditions for the catalyst preparation and the chemical interaction between nickel and the support [16–18]. Among these factors, types of the support are important to improve the DRM activity and stability of Ni catalysts [18–20]. Currently, many oxide supported Ni such as Ni/γ-Al_2O_3 [21], Ni/SiO_2 [22], and Ni/La_2O_3 [23] have been investigated. For Ni/Al_2O_3 and Ni/SiO_2, both CH_4 and CO_2 were activated on the same metal active sites as proposed by mono-functional mechanism and therefore the reaction rates were decreased [24]. On the other hand, the bi-functional mechanism was proposed for the Ni/La_2O_3 catalyst. The CH_4 dissociation occurred on Ni nanoparticles whereas the CO_2 activation occurred on La_2O_3 support [25]. The $La_2O_2CO_3$ phase was formed by reaction of the CO_2 reactant and the La_2O_3 support. The Ni/γ-Al_2O_3 and Ni/La_2O_3 catalysts were compared in the work of Al-Fatesh *et al.* [21]. They speculated that the Ni/La_2O_3 catalyst showed higher stability during the DRM for a long time because the formation of $La_2O_2CO_3$ phase enhanced the adsorption of CO_2. The $La_2O_2CO_3$ phase can also inhibit coke formation by the creation of carbonates or oxycarbonates during the reaction [26]. However, a main problem of the Ni/La_2O_3 catalyst was poor dispersion of active Ni metals on the La_2O_3 due to low surface area [27]. In order to solve this problem, mineral-type precursor was introduced into the support to obtain high Ni dispersion through the formation of special structure [28–30]. Examples of this structure were perovskite [17], spinel [31], and fluorite [32]. Numerous research works have been published regarding high activity and stability for the DRM on the $LaNiO_3$ perovskite materials [33–35]. Oliveira *et al.* [33] reported the synthesis of a $LaNiO_3$ perovskite by a single step using chitosan as a chelating agent. This method showed the formation of 95% of the $LaNiO_3$ phase. They found that this catalyst showed high CH_4 and CO_2 conversions and good yields of CO and H_2. Chiarello *et al.* [36] reported the preparation of a $LaCoO_3$ perovskite by a single step FSP synthesis. The mechanism of perovskite formation by the FSP method was dependent on system condition, solvent volatility and lattice energies. These affected structure, particle size, thermal stability temperature [36,37]. Moreover, the $LaCoO_3$ perovskite structure can be modified by substitution of transition metals (Zn, Cu, Fe, Cr, Mn, or others) for Co sites. The transition metals have variable oxidation states and therefore they can change the oxygen mobility within the crystal lattice of the supported catalyst [38,39]. Touahra *et al.* [40] studied cooperation of Ni metal and $LaCuO_3$ perovskite support for the DRM. The $LaCuO_3$ perovskite supported NiO catalyst showed high catalytic activity and stability during the DRM compared to a $LaCuO_3$ perovskite catalyst. From the above information, we are interested in the mixed oxides consisting of the transition metals and La_2O_3 to be the catalyst support for the DRM. In this work, four transition metals Co, Mn, Zn and Cu were studied. This catalyst supports were synthesized by the flame spray pyrolysis (FSP). The Ni-based catalyst supported on the FSP-made material was evaluated in the DRM.

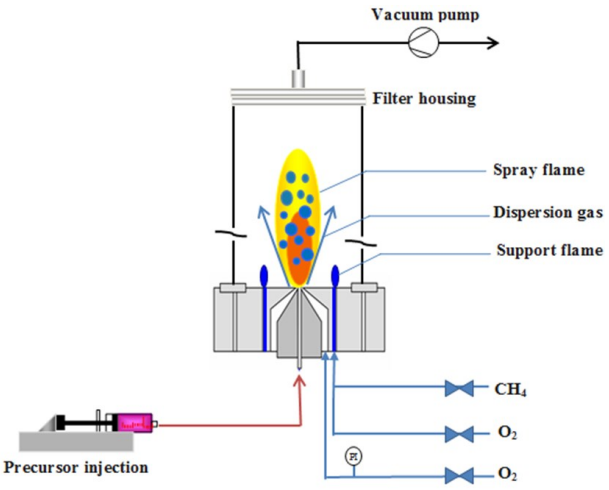

Figure 1. Scheme of equipment of flame spray pyrolysis (FSP).

2. Materials and Methods

2.1 Material Preparation

The support material consisting of transition metal and lanthanum was synthesized by flame spray pyrolysis. The FSP equipment is shown in Figure 1. The precursors of four transition metals were cobalt(II) nitrate hexahydrate ($Co(NO_3)_2.6H_2O$), manganese(II) nitrate tetrahydrate ($Mn(NO_3)_2.4H_2O$), copper(II) nitrate trihydrate ($Cu(NO_3)_2.3H_2O$) and zinc nitrate hexahydrate ($Zn(NO_3)_2.6H_2O$). The lanthanum(III) nitrate hexahydrate ($LaN_3O_9.6H_2O$) was used as the precursor of lanthanum. Both precursors were diluted by ethanol and fed into the center of a CH_4/O_2 flame using a syringe. The fine spray was formed by a capillary tip and evaporated into the flame. The dispersed oxygen was used in order to ensure the complete oxidation during the FSP step. The support material was collected on a glass microfiber filter with the aid of a vacuum pump. The Ni-based catalyst was prepared by incipient wetness impregnation (IWI). The nickel nitrate ($Ni(NO_3)_2$) aqueous solution was impregnated into the FSP-made support. The Ni loading was fixed as 2 wt%. The sample was kept at ambient temperature for 6 h and then dried at 110 °C for 12 h. Finally, the catalyst was calcined in air flow at 800 °C for 4 h. This catalyst was addressed as Ni/X-La_2O_3 when X symbol was transition metal (X = Co, Mn, Cu or Zn). The 30 wt% of transition metal based on the whole support was fixed in this work.

2.2 Material Characterization

The XRD measurement was used for identification and quantification of minerals, compounds and other crystalline phases of the catalyst. It was conducted on X-ray diffractometer SIEMENS D-5000 with a Cu Kα radiation source. The intensity data was recorded over a 2θ range of 20°–80° with a step size of 0.01° and with a scanning rate of 2°/min.

The specific surface area and the pore characteristics of the catalyst were determined by N_2 physisorption. The BET measurement was performed by BELSORP MINI II. Before the measurement, the catalyst was pretreated using He gas flow. The volume of adsorbed N_2 was measured at −196 °C using the different N_2 partial pressure.

The relative amount of active metals on the catalyst surface was estimated by H_2 chemisorption technique using a Micromeritics Pulse Chemisorb 2910 instrument. A 0.1 g of the catalyst sample was placed in a quartz U-shape reactor. Before the chemisorption step, the catalyst was reduced at 500 °C for 2 h. A 100 µl of the H_2 gas was injected into the catalyst at room temperature until saturation. The metal active sites were calculated from the volume of H_2 injected into the catalyst.

The reduction behavior of the catalyst was investigated by temperature programmed reduction with H_2 (H_2-TPR) using a Micrometritics Pulse Chemisorb 2910 instrument. A 0.1 g of the catalyst sample in a quartz U-shape reactor was reduced under a 30 ml/min of 10% H_2/N_2 gas flow from 100 to 800 °C. The water produced during the reduction was trapped by the liquid nitrogen.

Thermogravimetric analysis (TGA) was performed by SDT Q600 equipment. The catalyst was heated from room temperature up to 1000 °C in a heating rate of 10 °C/min under an air flow to measure loss of the catalyst weight.

2.3 Material Testing

The catalyst material was evaluated by the DRM. This reaction was occurred in a quartz tubular reactor under atmospheric pressure. A 0.3 g of the catalyst was packed in this reactor. The gas reactant was CH_4 and CO_2 with a molar ratio of unity. Prior to the catalytic testing, the temperature was raised to 500 °C in Ar flow and then the catalyst was reduced by H_2 flow at 500 °C for 2 h. After the reduction, the reactor temperature was increased to 700 °C in Ar flow and the gas reactant with GHSV of 18,000 h^{-1} was introduced. The composition of the outlet stream was analyzed by gas chromatograph (GC) using Porapak Q column connecting with TCD detector. The catalytic activity and the product yield were reported to show the catalytic performance in the DRM. The CH_4 and CO_2 conversions, H_2/CO ratio, and H_2 yield were calculated by formulae as follows:

$$CH_4\ conversion\,(\%) = \frac{mole\,of\,CH_{4,in} - mole\,of\,CH_{4,out}}{mole\,of\,CH_{4,in}} \times 100 \quad (5)$$

$$CO_2\ conversion\,(\%) = \frac{mole\,of\,CO_{2,in} - mole\,of\,CO_{2,out}}{mole\,of\,CO_{2,in}} \times 100 \quad (6)$$

$$H_2\ yield\ (\%) = \frac{mole\ of\ H_{2,out}}{2 \times mole\ of\ CH_{4,in}} \times 100 \quad (7)$$

$$H_2/CO\ ratio = \frac{mole\ of\ H_{2,out}}{mole\ of\ CO_{out}} \quad (8)$$

3. Results and Discussion

3.1 The Roles of Transition Metal in the Ni-based Catalysts

The physical, chemical and catalytic properties of this catalyst are reported. The crystalline structure of the synthesized catalyst materials was investigated by X-ray diffractometer as shown in Figure 2. It was found that the Ni/Co-La_2O_3 and Ni/Mn-La_2O_3 catalysts showed the perovskite structure of $LaCoO_3$ and $LaMnO_3$, respectively [41,42]. This confirmed that the FSP method can be an efficient way to produce the perovskite-structure material. The Mn and La metals can easily form this structure consistent with the literatures [43,44]. A rapid quench at high temperature during flame process helped in an interaction between two metal oxides of the support and an maintenance of vacancies in the perovskite structure [45].

Schematic illustration of an example of the formation of $LaCoO_3$ perovskite structure during the FSP process is shown in Figure 3. As a high resolution of the XRD main peak between 31° and 35° (2θ scale) for the Ni/Co-La_2O_3 and Ni/Mn-La_2O_3 catalysts shown in Figure 4(a), the position of the main peak of the Ni/Mn-La_2O_3 was shifted more than that of the Ni/Co-La_2O_3 due to the valance change of some Mn cation from +3 to +4. The unusual oxidation states were a mixture Mn^{3+}/Mn^{4+} ions with higher Mn^{3+} content. This indicated that the Ni/Co-La_2O_3 created the rhombohedral perovskite while the Ni/Mn-La_2O_3 showed a mixture of orthorhombic and rhombohedral perovskite [44,46]. As shown in Figure 2, the Ni/Cu-La_2O_3 showed narrow peaks of La_2CuO_4 spinel and CuO phase matching well with the reported data in literature [31]. The La_2CuO_4 (LaO+$LaCuO_3$) spinel belonged to the perovskite family, which the A site (La^{3+}) had a larger metal cation than the B site (Cu^{2+}). The La_2CuO_4 spinel, a mixture of LaO and $LaCuO_3$, belonged to the perovskite family, which the A site (La^{3+}) had a larger metal cation than the B site (Cu^{2+}). This structure had a lot of attention as a superconducting material [47,48]. When the zinc was introduced into the FSP-made support, a mixed phase of La_2O_3, ZnO and $La(OH)_3$ was apparent. It was indicated that Zn was inconstant in the perovskite structure under these conditions. The work by Moradi *et*

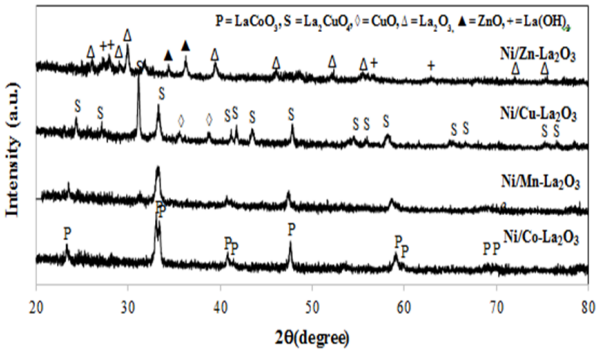

Figure 2. XRD patterns of Ni/Co-La_2O_3, Ni/Mn-La_2O_3, Ni/Cu-La_2O_3 and Ni/Zn-La_2O_3 catalysts.

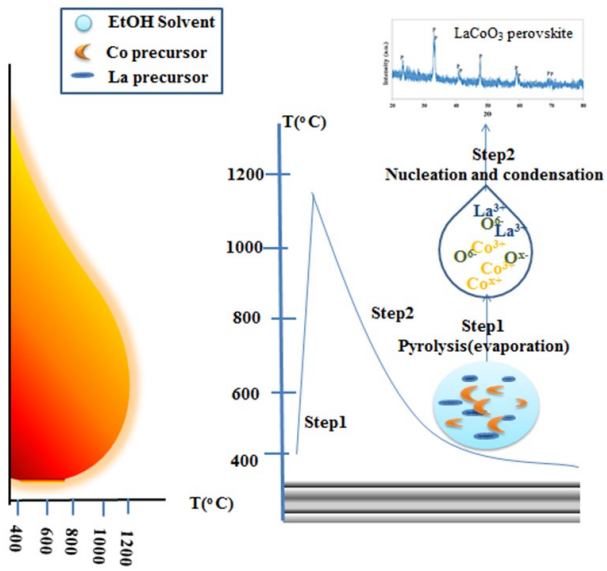

Figure 3. Schematics illustration of Co-La_2O_3 catalyst by FSP.

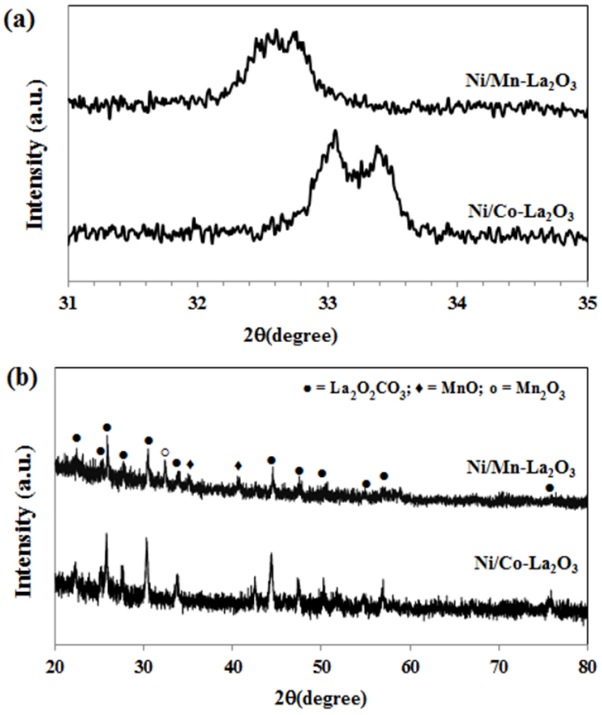

Figure 4. XRD patterns of Ni/Co-La_2O_3, Ni/Mn-La_2O_3, Ni/Cu-La_2O_3 and Ni/Zn-La_2O_3 catalysts; (a) more intense peaks and (b) after catalytic test at 700 °C for 15 h.

al. [49] reported the formation $LaNiO_3$ rhombohedra structure of $LaNi_{0.8}Zn_{0.2}O_3$ catalyst. When increasing the Zn loading by 0.6, it showed the three phases instead of the perovskite structure ($LaNiO_3$), which corresponded to the lanthanum oxide (La_2O_3), nickel lanthanum oxide (La_2NiO_4) and zinc oxide (ZnO) phases. Figure 4(b) shows the XRD patterns of the Ni/Co-La_2O_3 and Ni/Mn-La_2O_3 catalysts after testing the DRM at 700 °C for 15 h. The $La_2O_2CO_3$ phase was clearly apparent because the La_2O_3 reacted with the CO_2 reactant during the DRM. It was also remarked that the Ni/Co-La_2O_3 spent catalyst showed very high intensity of the XRD peak. The $La_2O_2CO_3$ phase could inhibit carbon formation on the catalyst surface [26]. Valderrama *et al*. [12] also reported that a mixed phase of $La_2O_2CO_3$, MnO and Mn_2O_3 was found on the Ni/Mn-La_2O_3.

Table 1 shows the data of N_2 physisorption and H_2 chemisorption. The BET surface area of four catalysts was in a range of 3.4–12.8 m^2/g. The Ni/Mn-La_2O_3 showed the highest surface area, which was close to the value of 11.0 m^2/g

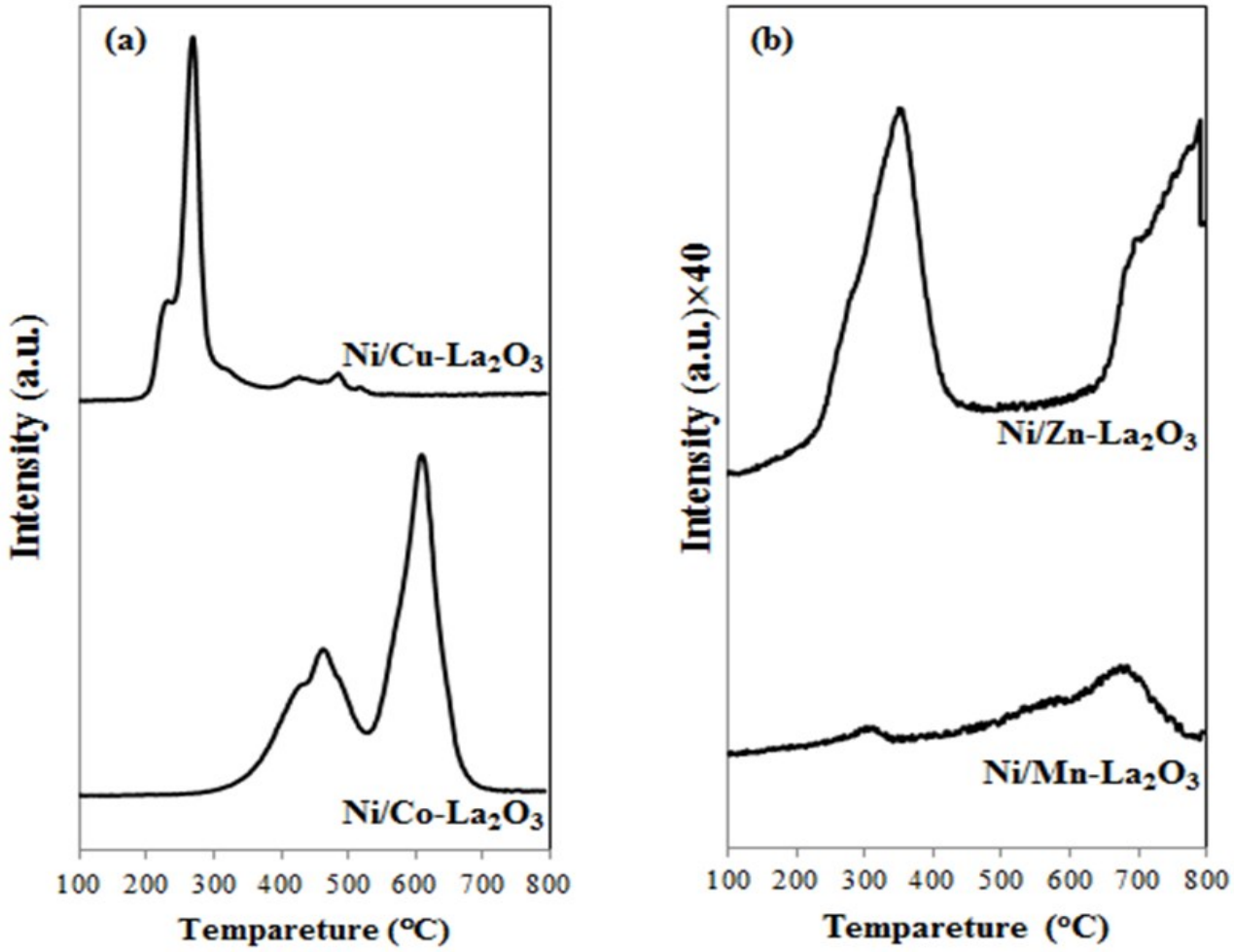

Figure 5. H_2-TPR profiles of (a) Ni/Co-La_2O_3 and Ni/Cu-La_2O_3 catalysts, (b) more intense peaks of Ni/Mn-La_2O_3 and Ni/Zn-La_2O_3 catalysts.

Table 1. The structure, BET surface area (S_{BET}), Pore volume and H_2 chemisorption of all catalysts.

Catalyst	Structure	S_{BET} (m^2/g)	Pore volume (cm^3/g)	H_2 chemisorption ($\times 10^{18}$ atom/g catalyst)
Ni/Co-La_2O_3	$LaCoO_3$ perovskite	3.4	0.005	13.3
Ni/Mn-La_2O_3	$LaMnO_3$ perovskite	12.8	0.075	4.8
Ni/Cu-La_2O_3	spinel	3.4	0.016	0.7
Ni/Zn-La_2O_3	La_2O_3, ZnO, $La(OH)_3$	8.4	0.036	1.2

reported in the other work [12]. The N_2 adsorption/desorption isotherm was not shown here. However, it was found that for four catalysts the same pattern of the typical type-II isotherms was identified. These isotherms were unrestricted monolayer-multilayer adsorption indicating the existence of non-porous or macro-porous characteristics [50]. The metal active sites of the catalysts were measured by H_2 chemisorption. It was found that the Ni/Co-La_2O_3 exhibited the highest active sites. It was notable that H_2 can chemisorb on both Co and Ni active sites. This indicated the dual-sites adsorption of Ni and Co metals. On the other hand, a small amount of chemisorbed H_2 on the three other catalysts was observed. This was well known that the H_2 was weakly chemisorbed on Mn and Cu metal sites and it was not absorbed on Zn metallic sites [51]. Therefore, the results of H_2 chemisorption for three catalysts were implied to the Ni metallic sites on the catalyst surface. An order of H_2 chemisorption of three catalysts related to the BET surface area of them. It was remarked that the Ni/Cu-La_2O_3 and Ni/Zn-La_2O_3 catalysts showed very low active sites. Jalali *et al*. [52] also reported that a large crystallite size of Ni metal was found on the Ni/$CuAl_2O_4$ and Ni/$ZnAl_2O_4$ catalysts.

The H_2-TPR profiles of all catalysts are presented in Figure 5. Because of very low intensity of H_2 consumption for the Ni/Mn-La_2O_3 and Ni/Zn-La_2O_3 catalysts, the TPR profile signal of these catalysts was adjusted to be 40 times of that of the Ni/Co-La_2O_3 and Ni/Cu-La_2O_3 catalysts. The Ni/Co-La_2O_3 exhibited the two reduction regions at below and above 520 °C. This was due to the reduction of NiO, Co_3O_4 and $LaCoO_3$. It was believed that the Co_3O_4 phase was present on the catalyst surface because the cobalt content in the catalyst was more than the stoichiometric ratio of the $LaCoO_3$ formation. Three steps of $LaCoO_3$ reduction were proposed by the other works [4,9,26] as shown in the following equations.

$$LaCoO_3 + 0.25H_2 \rightarrow LaCoO_{2.75} + 0.25H_2O \quad (9)$$
$$4LaCoO_{2.75} + H_2 \rightarrow La_4Co_3O_{10} + Co + H_2O \quad (10)$$
$$La_4Co_3O_{10} + 4H_2 \rightarrow 2La_2O_3 + 3Co + 4H_2O \quad (11)$$

At below 520 °C, the results could be attributed to the reduction of NiO to metallic Ni with concomitant formation of $LaCoO_{2.75}$ and $La_4Co_3O_{10}$ from Equations (9) and (10), respectively. It was noted that the reduction temperature of a bulk NiO was normally about 350 °C. At above 520 °C, the reduction by Equation (11) was proposed to represent a strong interaction between metallic Co and La_2O_3 support. However, it was unclear about the reduction temperature of Co_3O_4 species. From the previous work [53], it was indicated that the Co_3O_4 formed by the FSP technique was reduced by H_2 in a wide temperature range of 150–750 °C. If the reduction by H_2 followed the Equations (9) and (10), the theoretical ratio of H_2 consumption at below and above 520 °C could be equal to 0.5. From the deconvolution of TPR profile, the ratio of H_2 consumption at low and high temperatures was about 0.4 and therefore it was possible that most of the Co_3O_4 were reduced at above 520 °C. The TPR profile of the Ni/Cu-La_2O_3 showed two reduction regions. The first region at below 300 °C indicated a sharp peak with a low-temperature shoulder. The very small broad peaks were observed in a high temperature range. All of the peaks in both regions could be attributed to the reduction of NiO, La_2CuO_4 and segregated CuO. The XRD results in Figure 2 confirmed the presence of two latter species. The CuO was generally reduced by two reduction steps at low temperatures [54]. It was possible that the CuO was first reduced to Cu_2O and then to Cu^0 in the first region. The reduction of La_2CuO_4 was explained by Velasquez *et al*. [55]. They proposed the partial reduction of La_2CuO_4 to form $LaCuO_{2+x}$ and Cu_2O at 230–320 °C and subsequently the $LaCuO_{2+x}$ and Cu_2O were reduced at 420–550 °C. This suggestion was coincident with our results. It was also postulated that some of H_2 consumption in the second region was obtained by the reduction of NiO to Ni^0.

The Ni/Mn-La_2O_3 and the Ni/Zn-La_2O_3 catalysts demonstrated very low intensity of H_2 consumption compared with the Ni/Co-La_2O_3 and the Ni/Cu-La_2O_3 catalysts. This was due to a difficult reduction of $LaMnO_3$ perovskite and ZnO. The Ni/Mn-La_2O_3 showed a main peak between 300–400 °C. It was clear that the reduction of NiO to Ni^0 was occurred in this temperature range. It was possible that the reduction of MnO_2 and some of $LaMnO_3$ perovskite-like structure was also occurred. Although the MnO_2 was not found by the XRD analysis as shown in Figure 2, it can be formed during the FSP step like the formation of Co_3O_4 in the Ni/Co-La_2O_3 as discussed above. At low temperature, the reduction of Mn^{4+} to Mn^{3+} was declared while the reduction of Mn^{3+} to Mn^{2+} was assigned at high temperatures [44]. These were consistent with the signal of H_2 consumption in a range of 300–400 °C and above 600 °C, respectively. The reduction of $LaMnO_3$ perovskites was a complex process. This occurred in a wide temperature range of 200–900 °C as

proposed by Valderrama *et al.* [12]. They suggested that La_2O_3, $La(OH)_3$ and MnO species were formed after the reduction of $LaMnO_{3.15}$. It was possible that the lanthanum manganite was also reduced in this work. The presence of MnO was confirmed by the XRD results of the spent catalysts as shown in Figure 4(b). It was indicated that the MnO obtained by H_2 reduction was stable under the reaction condition. Besides, the appearance of the Mn_2O_3 phase in the spent catalyst exhibited the reduction of either MnO_2 species or other forms of perovskites such as the $La_{0.93}MnO_3$ structure proposed by the literature [12]. In the case of Ni/Zn-La_2O_3, a very small reduction peak at 300 °C was implied as the reduction of NiO to Ni^0. The results of the H_2 chemisorption form Table 1 and this TPR profile indicated a very small amount of Ni metallic sites on the catalyst surface. It was possible that in this case some of nickel and ZnO could generate the NiZn alloy during the preparation of the catalyst although this alloy was not found by the XRD. The reduction peak at above 500 °C was attributed the reduction of ZnO to metallic zinc [56] or the NiO interacted strongly with ZnO in the NiZn alloy [57].

The four catalysts were evaluated by the DRM reaction at 700 °C for 15 h. The CH_4 conversion and the molar ratio of H_2 and CO in the product were plotted with time on stream as shown in Figure 6. The reaction behaviors of the Ni/Co-La_2O_3 were different from the three other catalysts. This was an increase of the catalytic activity of the Ni/Co-La_2O_3 with increasing time during 1–7 h. Before the reaction test, this catalyst was reduced by H_2 at 500 °C for 2 h. At this temperature, the reduction of the $La_4Co_3O_{10}$ and some Co_3O_4 strongly interacted with the support was incomplete as confirmed by the TPR results in Figure 5(a). Hence, during the DRM reaction at 700 °C, the $La_4Co_3O_{10}$ and Co_3O_4 species were gradually reduced by the H_2 produced from the reaction resulting in an increase of metallic active cobalt sites on the catalyst surface. The complete reduction was expected in 7 h and a change of CH_4 conversion was significantly observed. After 7 h, for all catalysts the CH_4 conversion and the H_2/CO ratio in the product stream remained constant indicating no deactivation due to coking. This was because the formation of $La_2O_2CO_3$ phase during the reaction test could inhibit carbon formation on the catalyst surface. The presence of this phase on the spent catalysts was confirmed by the XRD results in Figure 4(b). Figure 7 shows the comparable results of the two reactant conversions and the H_2 product yield of the DRM reaction at 700 °C for 15 h. For all four catalysts, the CO_2 reactant was converted more than the CH_4 indicating an occurrence of the reverse water-gas shift reaction (RWGS). Hence, the obtained H_2/CO molar ratios were lower than the stoichiometric ratio. The Ni/Co-La_2O_3 exhibited the highest conversions, H_2 product yield and H_2/CO product ratio. It was noted that the catalytic activity of the Co-La_2O_3 support was also collected but not shown here. This support showed less than 10% of both CH_4 and CO_2 conversions. Therefore, a cooperative effect of the Ni and Co metal active sites on the La_2O_3 matrix was nec-

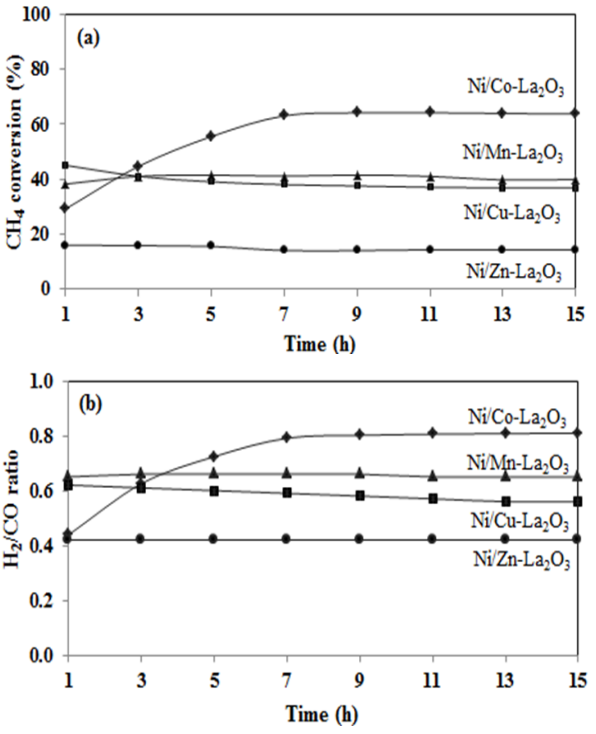

Figure 6. (a) CH_4 conversion and (b) H_2/CO ratio of Ni/Co-La_2O_3, Ni/Mn-La_2O_3, Ni/Cu-La_2O_3 and Ni/Zn-La_2O_3 catalysts in DRM at 700 °C for 15 h.

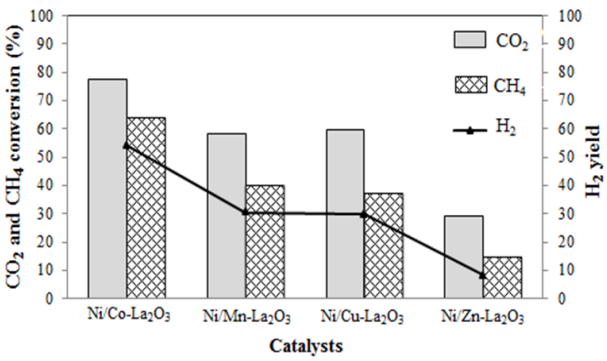

Figure 7. CH_4 and CO_2 conversions and H_2 yield of Ni/Co-La_2O_3, Ni/Mn-La_2O_3, Ni/Cu-La_2O_3 and Ni/Zn-La_2O_3 catalysts in DRM at 700 °C, 15 h.

essary to activate the reactant in this case. The Ni/Mn-La_2O_3 and Ni/Cu-La_2O_3 catalysts showed moderate catalytic activity in the same level. However, the different mechanisms were proposed. For the Ni/Mn-La_2O_3, the metal active sites were only dispersed metallic Ni particles. The Mn and La species were in oxide forms. It was speculated that the segregated Mn_2O_3 and MnO with small particle size retarded agglomeration of impregnated Ni resulting in a high dispersion of Ni active sites measured by H_2 chemisorption as shown in Table 1. The Ni metal, MnO particle and La_2O_3 support was key components to activate the CH_4 and CO_2 reactants for the DRM reaction in this case. The MnO can react with CO_2 to produce MnO_2 and CO [58]. In addition, the carbon deposits can be also removed by the MnO_2 as shown in the following Equations (12) and (13) [59]:

$$CO_2 + MnO \rightarrow CO + MnO_2 \quad (12)$$

$$C + MnO_2 \rightarrow CO + MnO \quad (13)$$

For the Ni/Cu-La_2O_3, a low amount of Ni active sites can maintain a promising catalytic activity. It was speculated that the Cu metal, which was obtained by the reduction of CuO at low temperatures, had an important role to activate CH_4 as well. In this case, the synergistic effect of Ni and Cu metals was a key factor to catalyze the DRM. The Ni/Zn-La_2O_3 showed the lowest activity due to a low amount of metallic Ni active sites. The ZnO on the catalyst surface was inactive to the DRM reaction. However, the presence of the NiZn alloy was expected to have a promotional effect on the activity and stability consistent with the work of Masoom Nataj *et al.* [60].

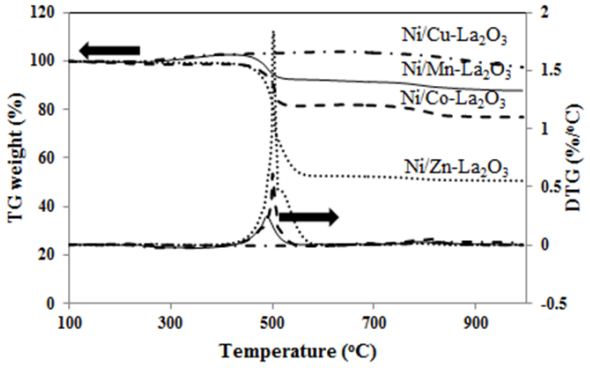

Figure 8. TG weight and DTG profile of Ni/Co-La_2O_3, Ni/Mn-La_2O_3, Ni/Cu-La_2O_3 and Ni/Zn-La_2O_3 spent catalysts in DRM at 700 °C for 15 h.

Figure 8 shows TG weight and DTG profiles of the spent catalysts under air flow. These catalysts were obtained from the DRM reaction test at 700 °C for 15 h. The TG results exhibited weight losses in two temperature ranges. As reported by Lima *et al.* [14], the weight loss in a range of 300 and 550 °C represented the oxidation of the carbon deposits while the weight loss at about 800 °C suggested the decomposition of La carbonates. The Ni/Zn-La_2O_3 presented the highest DTG intensity and TG weight loss at 49.5% as shown in Table 2. This implied high amount of coke on the catalyst surface affecting very low activity. The Ni/Mn-La_2O_3 showed the TG weight loss lower than the Ni/Co-La_2O_3. From the XRD results in Figure 4(b), the mixed phases of $La_2O_2CO_3$, MnO and Mn_2O_3 were present in the Ni/Mn-La_2O_3. Besides the $La_2O_2CO_3$, the MnO species can remove the carbon deposits on the catalyst surface as shown above in Equations (12) and (13). While the coke formation on the Ni/Co-La_2O_3 catalyst was inhibited by only $La_2O_2CO_3$ species. The Ni/Cu-La_2O_3 showed a small amount of coke on the catalyst surface. An increase of TG weight in a wide range of temperature was due to the re-oxidation of Cu^+ to Cu^{2+}, which occurred at a temperature of 300–700 °C [17]. The weight loss in the temperature range of 750–1000 °C was the carbonaceous deposits and presented 2.6 wt.% [55].

3.2 The Partial Substitution of Co for Mn into the Ni/Co-La_2O_3 Catalyst

The Ni/Co-La_2O_3 was a promising candidate to catalyze the DRM. It showed high product yield of H_2 and had no deactivation in 15 h. However, a significant amount of carbon deposits reported by the above TG results may possibly cause deactivation by prolonging the reaction time. To solve this problem, it was interesting to study the partial substitution of Co for Mn because the MnO can remove the carbon on the catalyst surface together with the $La_2O_2CO_3$ as discussed above. In this case, the

Table 2. The weight loss of spent catalysts in DRM at 700 °C for 15 h.

Catalyst	Weight loss TG after reaction (%)
Ni/Co-La_2O_3	23.2
Ni/Mn-La_2O_3	12.3
Ni/Cu-La_2O_3	2.6
Ni/Zn-La_2O_3	49.5

Co, Mn and La precursors were simultaneously fed into the flame to synthesize the FSP-made supports. These supports were addressed as Mn_xCo_{1-x}-La_2O_3 when x meant a molar fraction of Mn in the mixture of Mn and Co. Three supports were synthesized in this work. Two of them were loaded by low Mn content (x = 0.05 and 0.1) and another was an equimolar mixture of Mn and Co. A 2 wt% Ni was loaded on the Mn_xCo_{1-x}-La_2O_3 support by incipient wetness impregnation method and then the Ni-based catalysts were calcined in air flow at 800 °C for 4 h. The X-ray diffraction spectra of samples with different Mn doping are shown in Figure 9. The X-ray diffraction spectra of three catalysts with co-doped Co and Mn are compared to those of the Ni/Co-La_2O_3 and Ni/Mn-La_2O_3 catalysts as shown in Figure 9(a). The partial substitution can maintain the perovskite-type structure consistent with the literatures [61,62]. The crystal spacing calculated by Bragg equation was slightly increased with increasing the Mn content. Figure 9(b) shows the different position of the XRD main peak at 32–34°. This was indicated that the Mn ion partly entered into the perovskite-type structure by replacing the Co ion. An increase of Mn-substitution amounts exhibited the peak shift to lower 2θ since the ionic radius of Mn^{3+} (0.645 Å) was larger than that of Co^{3+} (0.545 Å). From the XRD results, it was also remarked that the coexistence of rhombohedral and orthorhombic phases was apparent in the Mn_xCo_{1-x}-La_2O_3 support dependent on the degree of Mn substitution [12,44].

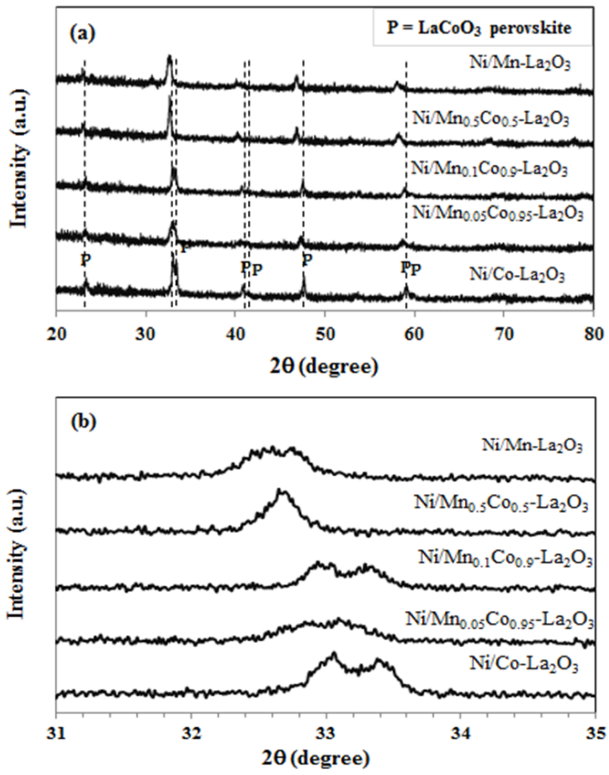

Figure 9. XRD patterns of Ni/Co-La_2O_3, Ni/$Mn_{0.05}Co_{0.95}$-La_2O_3, Ni/$Mn_{0.1}Co_{0.9}$-La_2O_3, Ni/$Mn_{0.5}Co_{0.5}$-La_2O_3 and Ni/Mn-La_2O_3 catalysts (a) as prepared and (b) more intense peaks.

Figure 10 shows the H_2-TPR profiles of the Ni/Mn_xCo_{1-x}-La_2O_3 catalysts. As compared to the Ni/Co-La_2O_3, the reduction peaks at below 520 °C were shifted to lower temperature and the area of these peaks was varied by the substituted Mn content. While a new broad reduction peak was apparent at above 700 °C. This was because Mn with high valence was inserted into the perovskite structure resulting the reduction of some Co^{3+} to Co^{2+} [46]. At low temperature, the Co_3O_4, MnO_2 and NiO particles formed during the FSP step and dispersed on the catalyst surface were mainly reduced. At high temperature, the reduction of lattice oxygen ion in the perovskite structure was proposed. It was speculated that the strength of Co–O–Co bond was weaken compared to Co–O–Mn and Mn–O–Mn bonds. This was implied that the reduction peak at 600 °C was attributed to Co–O–Co bond while the broad peak at above 650 °C was related to Co–O–Mn and Mn–O–Mn bonds. From the TPR results, it was implied that the Ni/$Mn_{0.05}Co_{0.95}$-La_2O_3 and Ni/$Mn_{0.5}Co_{0.5}$-La_2O_3 catalysts showed more Co–O–Co and more Co–O–Mn bonds, respectively, while the Ni/$Mn_{0.1}Co_{0.9}$-La_2O_3 consisted of both Co–O–Co and Co–O–Mn within the crystal lattice. It was also noted that the Ni/$Mn_{0.1}Co_{0.9}$-La_2O_3 catalyst showed a high amount of reduced H_2. This was possible that more Mn entered into the perovskite structure and therefore excess Co became more Co_3O_4 particles dispersed on the catalyst surface. The

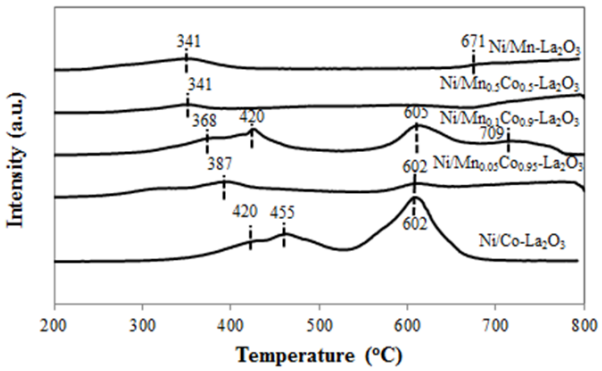

Figure 10. TPR profiles of Ni/Co-La_2O_3, Ni/$Mn_{0.05}Co_{0.95}$-La_2O_3, Ni/$Mn_{0.1}Co_{0.9}$-La_2O_3, Ni/$Mn_{0.5}Co_{0.5}$-La_2O_3 and Ni/Mn-La_2O_3 catalysts.

Co_3O_4 formed during the FSP step can be reduced at both low and high temperatures [53].

The results of DRM reaction at 700 °C for 15 h were reported in Figures 11 and 12. It was found that the Ni/$Mn_{0.05}Co_{0.95}$-La_2O_3 catalyst showed the highest CH_4 conversion, H_2 yield and H_2/CO ratio. This catalyst can maintain the activity and product yield for 15 h. This was suitable content of Mn inserted into the perovskite structure to change the oxygen mobility within the crystal lattice of the Co component. Both the Ni/$Mn_{0.1}Co_{0.9}$-La_2O_3 and the Ni/$Mn_{0.5}Co_{0.5}$-La_2O_3 catalysts showed a significant decrease of the CH_4 conversion. A large amount of Co_3O_4 particles in the Ni/$Mn_{0.1}Co_{0.9}$-La_2O_3 catalyst confirmed by the TPR result was possible to accelerate the coke formation and therefore the DRM activity was dropped. On the other hand, for the Ni/$Mn_{0.5}Co_{0.5}$-La_2O_3 catalyst more Co−O−Mn bond in the crystal lattice can inhibit the formation of $La_2O_2CO_3$ phase resulting in high propagation rate of carbon. It was remarked that, low performance of the Ni/Mn-La_2O_3 catalyst was due to the distortion of non-rhombohedral perovskite symmetry and the effect of the reverse water-gas shift reaction [63].

Figure 13 shows the XRD signal of the spent catalysts. The $La_2O_2CO_3$ phase was apparent due to the La_2O_3 reacting with the CO_2 reactant during the DRM. This phase can inhibit carbon formation and improve the catalytic activity and stability of the DRM reaction [3,64,65]. The highest intensity of the $La_2O_2CO_3$ phase was found by the Ni/Co-La_2O_3 catalyst. The segregated Co_3O_4 phase was formed on the catalyst surface of the Ni/$Mn_{0.05}Co_{0.95}$-La_2O_3 catalyst. This was because the Co metal ion was substituted for Mn metal ion. However, the MnO_x phase disappeared due to a low amount of Mn. The Ni/$Mn_{0.1}Co_{0.9}$-La_2O_3 and the Ni/$Mn_{0.5}Co_{0.5}$-La_2O_3 catalysts show only $La_2O_2CO_3$ phase but lower intensity of XRD peaks.

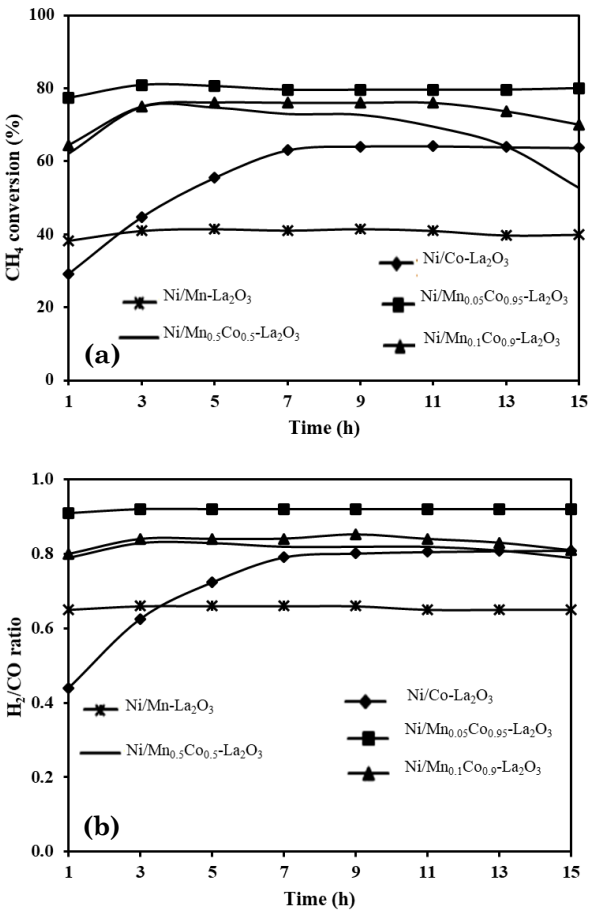

Figure 11. (a) CH_4 conversion and (b) H_2/CO ratio of Ni/Co-La_2O_3, Ni/$Mn_{0.05}Co_{0.95}$-La_2O_3, Ni/$Mn_{0.1}Co_{0.9}$-La_2O_3, Ni/$Mn_{0.5}Co_{0.5}$-La_2O_3 and Ni/Mn-La_2O_3 catalysts in dry reforming of methane at 700 °C for 15 h.

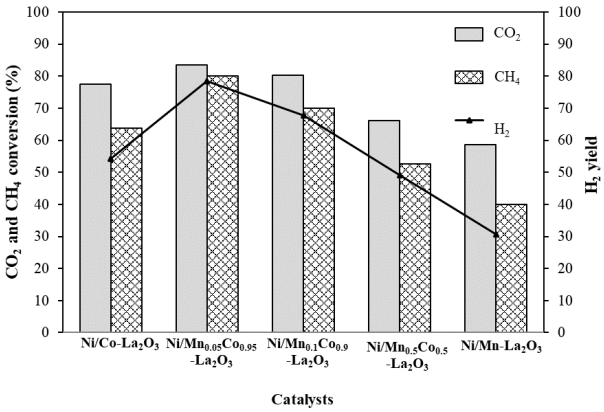

Figure 12. CH_4 and CO_2 conversion and H_2 yield of Ni/Co-La_2O_3, Ni/$Mn_{0.05}Co_{0.95}$-La_2O_3, Ni/$Mn_{0.1}Co_{0.9}$-La_2O_3, Ni/$Mn_{0.5}Co_{0.5}$-La_2O_3 and Ni/Mn-La_2O_3 catalysts in DRM at 700 °C, 15 h.

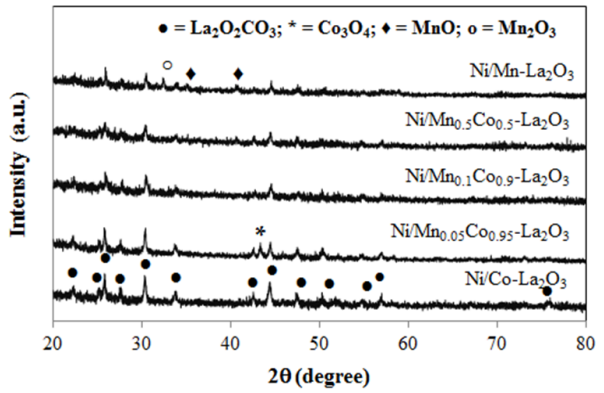

Figure 13. XRD patterns of Ni/Co-La_2O_3, Ni/$Mn_{0.05}Co_{0.95}$-La_2O_3, Ni/$Mn_{0.1}Co_{0.9}$-La_2O_3, Ni/$Mn_{0.5}Co_{0.5}$-La_2O_3 and Ni/Mn-La_2O_3 catalysts. after test catalytic at 700 °C for 15 h.

Figure 14 and Table 3 show the TG and DTG results of the spent catalysts after testing the dry reforming of methane at 700 °C for 15 h. These results indicated a significant amount of carbon deposits on the catalyst surface through the TG peak in a range of 300–550 °C. As discussed above, both $La_2O_2CO_3$ and MnO phases can inhibit the coke formation and therefore the Ni/Co-La_2O_3 and Ni/Mn-La_2O_3 catalysts showed a low amount of carbon deposits. For the same reason, the Ni/$Mn_{0.05}Co_{0.95}$-La_2O_3 catalyst had low rate of coke formation. More dispersed Co_3O_4 particles confirmed by the TPR results accelerated the propagation of coke on the surface of the Ni/$Mn_{0.1}Co_{0.9}$-La_2O_3 catalyst. For the Ni/$Mn_{0.5}Co_{0.5}$-La_2O_3 catalyst, much more Mn inserted into the perovskite structure can generate more Co–O–Mn bond in the lattice leading to the difficult formation of $La_2O_2CO_3$ phase. A high rate of coke formation in both Ni/$Mn_{0.1}Co_{0.9}$-La_2O_3 and Ni/$Mn_{0.5}Co_{0.5}$-La_2O_3 catalysts from the TG and DTG results was related to a decrease of the DRM activity with time on stream as shown above.

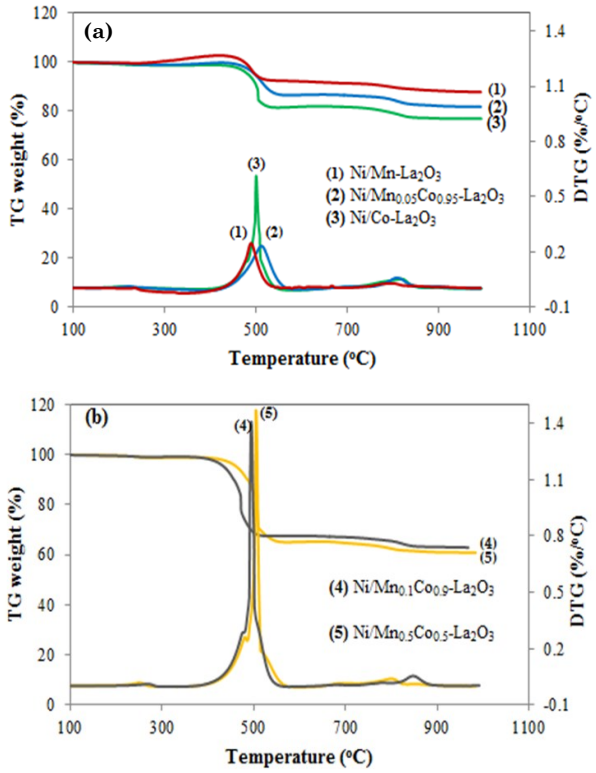

Figure 14. TG and DTG profile of Ni/Co-La_2O_3, Ni/$Mn_{0.05}Co_{0.95}$-La_2O_3, Ni/$Mn_{0.1}Co_{0.9}$-La_2O_3, Ni/$Mn_{0.5}Co_{0.5}$-La_2O_3 and Ni/Mn-La_2O_3 spent catalysts in dry reforming of methane at 700 °C for 15 h.

4. Conclusions

The Ni catalysts supported on the FSP-made transition metal (Co, Mn, Cu or Zn) doped La_2O_3 materials were investigated. It was found that the Ni/Co-La_2O_3 and Ni/Mn-La_2O_3 catalysts showed the $LaCoO_3$ and $LaMnO_3$ perovskites, respectively. This confirmed that the FSP method can be efficient to produce the perovskite-structure material. The Ni/Co-La_2O_3 created the rhombohedral perovskite while the Ni/Mn-La_2O_3 showed a mixture of orthorhombic and rhombohedral perovskites. The La_2CuO_4 spinel and CuO phase was apparent in the Ni/Cu-La_2O_3 while a mixed phase of La_2O_3, ZnO and $La(OH)_3$ was observed in the Ni/Zn-La_2O_3. High reducibility for the Ni/Co-La_2O_3 and Ni/Cu-La_2O_3 catalysts was related to the reduction of $LaCoO_3$ and La_2CuO_4 phases. High activity for the DRM reaction on the Ni/Co-La_2O_3 was due to a cooperative effect of the Ni and Co metal active sites on the La_2O_3 matrix. A high dispersion of metallic Ni particles on the surface of the Ni/Mn-La_2O_3 and the dual sites of Ni and Cu on the Ni/Cu-La_2O_3 resulted in moderate DRM activity. On the other hand, the Ni/Zn-La_2O_3 showed low DRM activity due to the agglomeration of the Ni particles on the catalyst surface. Among four catalysts, the Ni/Mn-La_2O_3 was promising catalyst to remove the carbon deposits through the cooperation of $La_2O_2CO_3$ and MnO_x. The partial substitution of Co for Mn with a small content of Mn enhanced the catalytic performance of the DRM reaction. The highest CH_4 conversion, H_2 yield and H_2/CO ratio were found in the Ni/$Mn_{0.05}Co_{0.95}$-La_2O_3 catalyst. However, an insertion of more Mn resulted in more Co being excluded from the perovskite structure and the Co_3O_4 particles was formed on the catalyst surface leading to acceleration of coke formation.

Table 3. The weight loss of Ni/Co-La_2O_3, Ni/$Mn_{0.05}Co_{0.95}$-La_2O_3, Ni/$Mn_{0.1}Co_{0.9}$-La_2O_3, Ni/$Mn_{0.5}Co_{0.5}$-La_2O_3 and Ni/Mn-La_2O_3 spent catalysts in dry reforming of methane at 700 °C for 15 h.

Catalyst	Weight loss TG after reaction (%)
Ni/Co-La_2O_3	23.2
Ni/$Mn_{0.05}Co_{0.95}$-La_2O_3	18.4
Ni/$Mn_{0.1}Co_{0.9}$-La_2O_3	36.7
Ni/$Mn_{0.5}Co_{0.5}$-La_2O_3	37.1
Ni/Mn-La_2O_3	12.3

Acknowledgment

The authors would like to thank Department of Chemical Engineering, Faculty of Engineering and Industrial Technology, Silpakorn University and Graduate School for financial support.

References

[1] Willard, D.A., Donders, T.H., Reichgelt, T., Greenwood, D.R., Sangiorgi, F., Peterse, F., Nierop, K.G., Frieling, J., Schouten, S., Sluijs, A. (2019). Arctic vegetation, temperature, and hydrology during Early Eocene transient global warming events. *Global and Planetary Change*, 178, 139-152. DOI: 10.1016/j.gloplacha.2019.04.012.

[2] Osazuwa, O.U., Setiabudi, H.D., Rasid, R.A., Cheng, C.K. (2017). Syngas production via methane dry reforming. A novel application of $SmCoO_3$ perovskite catalyst. *Journal of Natural Gas Science and Engineering*, 37, 435-448. DOI: 10.1016/j.jngse.2016.11.060.

[3] Sutthiumporn, K., Maneerung, T., Kathiraser, Y., Kawi, S. (2012). CO_2 dry-reforming of methane over $La_{0.8}Sr_{0.2}Ni_{0.8}M_{0.2}O_3$ perovskite (M=Bi, Co, Cr, Cu, Fe): Roles of lattice oxygen on C-H activation and carbon suppression. *International Journal of Hydrogen Energy*, 37, 11195-11207. DOI: 10.1016/j.ijhydene.2012.04.059.

[4] Arora, S., Prasad, R. (2016). An overview on dry reforming of methane: strategies to reduce carbonaceous deactivation of catalysts. *RSC Advances*, 6, 108668-108688. DOI: 10.1039/C6RA20450C.

[5] Aramouni, N.A.K., Touma, J.G., Tarboush, B.A., Zeaiter, J., Ahmad, M.N. (2018). Catalyst design for dry reforming of methane: analysis review. *Renewable and Sustainable Energy Reviews*, 82, 2570-2585. DOI: 10.1016/j.rser.2017.09.076.

[6] Budiman, A.W., Song, S.-H., Chang, T.-S., Shin, C.-H., Choi, M.-J.(2012). Dry reforming of methane over cobalt catalysts: a literature review of catalyst development. *Catalysis Surveys from Asia*, 16, 183-197. DOI: 10.1007/s10563-012-9143-2.

[7] Kathiraser, Y., Oemar, U., Saw, E.T., Li, Z., Kawi, S. (2015). Kinetic and mechanistic aspects for CO_2 reforming of methane over Ni based catalysts. *Chemical Engineering Journal*, 278, 62-78. DOI: 10.1016/j.cej.2014.11.143.

[8] Dama, S., Ghodke, S.R., Bobade, R., Gurav, H.R., Chilukuri, S. (2018). Active and durable alkaline earth metal substituted perovskite catalysts for dry reforming of methane. *Applied Catalysis B: Environmental*, 224, 146-158. DOI: 10.1016/j.apcatb.2017.10.048.

[9] Valderrama, G., de Navarro, C.U., Goldwasser, M.R. (2013). CO_2 reforming of CH_4 over Co–La-based perovskite-type catalyst precursors. *Journal of Power Sources*, 234, 31-37. DOI: 10.1016/j.jpowsour.2013.01.142.

[10] Ay, H., Üner, D. (2015). Dry reforming of methane over CeO_2 supported Ni, Co and Ni-Co catalysts. *Applied Catalysis B: Environmental*, 179, 128-138. DOI: 10.1016/j.apcatb.2015.05.013.

[11] Royer, S., Duprez, D., Can, F., Courtois, X., Batiot-Dupeyrat, C., Laassiri, S., Alamdari, H. (2014). Perovskites as substitutes of noble metals for heterogeneous catalysis: dream or reality. *Chemical Reviews*, 114, 10292-10368. DOI: 10.1021/cr500032a.

[12] Valderrama, G., Kiennemann, A., de Navarro, C.U., Goldwasser, M.R. (2018). $LaNi_{1-x}Mn_xO_3$ perovskite-type oxides as catalysts precursors for dry reforming of methane. *Applied Catalysis A: General*, 565, 26-33. DOI: 10.1016/j.apcata.2018.07.039.

[13] Abasaeed, A.E., Al-Fatesh, A.S., Naeem, M.A., Ibrahim, A.A., Fakeeha, A.H. (2015). Catalytic performance of CeO_2 and ZrO_2 supported Co catalysts for hydrogen production via dry reforming of methane. *International Journal of Hydrogen Energy*, 40, 6818-6826. DOI: 10.1016/j.ijhydene.2015.03.152.

[14] Lima, S., Assaf, J., Pena, M., Fierro, J. (2006). Structural features of $La_{1-x}Ce_xNiO_3$ mixed oxides and performance for the dry reforming of methane. *Applied Catalysis A*, 311, 94-104. DOI: 10.1016/j.apcata.2006.06.010.

[15] Rivas, I., Alvarez, J., Pietri, E., Pérez-Zurita, M.J., Goldwasser, M.R. (2010). Perovskite-type oxides in methane dry reforming: Effect of their incorporation into a mesoporous SBA-15 silica-host. *Catalysis today*, 149, 388-393. DOI: 10.1016/j.cattod.2009.05.028.

[16] Sokolov, S., Kondratenko, E.V., Pohl, M.-M., Rodemerck, U. (2013). Effect of calcination conditions on time on-stream performance of Ni/La_2O_3-ZrO_2 in low-temperature dry reforming of methane. *International Journal of Hydrogen Energy*, 38, 16121-16132. DOI: 10.1016/j.ijhydene.2013.10.013.

[17] Nair, M.M., Kaliaguine, S., Kleitz, F. (2014). Nanocast $LaNiO_3$ perovskites as precursors for the preparation of coke-resistant dry reforming catalysts. *Acs Catalysis*, 4, 3837-3846. DOI: 10.1021/cs500918c.

[18] Titus, J., Goepel, M., Schunk, S., Wilde, N., Gläser, R. (2017). The role of acid/base properties in Ni/MgO-ZrO_2–based catalysts for dry reforming of methane. Catalysis Communications, 100, 76-80. DOI: 10.1016/j.catcom.2017.06.027.

[19] Albarazi, A., Gálvez, M.E., Da Costa, P. (2015). Synthesis strategies of ceria–zirconia doped Ni/SBA-15 catalysts for methane dry reforming. *Catalysis Communications*, 59, 108-112. DOI: 10.1016/j.catcom.2014.09.050.

[20] Sokolov, S., Kondratenko, E.V., Pohl, M.-M., Barkschat, A., Rodemerck, U. (2012). Stable low-temperature dry reforming of methane over mesoporous La_2O_3-ZrO_2 supported Ni catalyst. *Applied Catalysis B: Environmental*, 113, 19-30. DOI: 10.1016/j.apcatb.2011.09.035.

[21] Al-Fatesh, A.S., Naeem, M.A., Fakeeha, A.H., Abasaeed, A.E. (2014). Role of La_2O_3 as promoter and support in Ni/γ-Al_2O_3 catalysts for dry reforming of methane. *Chinese Journal of Chemical Engineering*, 22, 28-37. DOI: 10.1016/S1004-9541(14)60029-X.

[22] Pompeo, F., Nichio, N.N., González, M.G., Montes, M. (2005). Characterization of Ni/SiO_2 and Ni/Li-SiO_2 catalysts for methane dry reforming. *Catalysis Today*, 107, 856-862. DOI: 10.1016/j.cattod.2005.07.024.

[23] Tsoukalou, A., Imtiaz, Q., Kim, S.M., Abdala, P.M., Yoon, S., Müller, C.R. (2016). Dry-reforming of methane over bimetallic Ni–M/La_2O_3 (M= Co, Fe): The effect of the rate of $La_2O_2CO_3$ formation and phase stability on the catalytic activity and stability. *Journal of Catalysis*, 343, 208-214. DOI: 10.1016/j.jcat.2016.03.018.

[24] Yan, X., DU, X.-h., Jing, L., Peng, W., Jie, Z., GE, F.-j., Jun, Z., Ming, S., ZHU, W.-y. (2019). A comparison of Al_2O_3 and SiO_2 supported Ni-based catalysts in their performance for the dry reforming of methane. *Journal of Fuel Chemistry and Technology*, 47, 199-208. DOI: 10.1016/S1872-5813(19)30010-6.

[25] Li, K., He, F., Yu, H., Wang, Y., Wu, Z. (2018). Theoretical study on the reaction mechanism of carbon dioxide reforming of methane on La and La_2O_3 modified Ni (1 1 1) surface. *Journal of Catalysis*, 364, 248-261. DOI: 10.1016/j.jcat.2018.05.026.

[26] Zhu, Q., Cheng, H., Zou, X., Lu, X., Xu, Q., Zhou, Z. (2015). Synthesis, characterization, and catalytic performance of $La_{0.6}Sr_{0.4}Ni_xCo_{1-x}O_3$ perovskite catalysts in dry reforming of coke oven gas. *Chinese Journal of Catalysis*, 36, 915-924. DOI: 1016/S1872-2067(14)60303-X.

[27] Li, X., Li, D., Tian, H., Zeng, L., Zhao, Z.-J., Gong, J. (2017). Dry reforming of methane over Ni/La_2O_3 nanorod catalysts with stabilized Ni nanoparticles. *Applied Catalysis B: Environmental*, 202, 683-694. DOI: 10.1016/j.apcatb.2016.09.071.

[28] Wang, H., Dong, X., Zhao, T., Yu, H., Li, M. (2019). Dry reforming of methane over bimetallic Ni-Co catalyst prepared from La$(Co_xNi_{1-x})_{0.5}Fe_{0.5}O_3$ perovskite precursor: Catalytic activity and coking resistance. *Applied Catalysis B: Environmental*, 245, 302-313. DOI: 10.1016/j.apcatb.2018.12.072.

[29] de Caprariis, B., de Filippis, P., Palma, V., Petrullo, A., Ricca, A., Ruocco, C., Scarsella, M. (2016). Rh, Ru and Pt ternary perovskites type oxides $BaZr_{(1-x)}Me_xO_3$ for methane dry reforming. *Applied Catalysis A: General*, 517, 47-55. DOI: 10.1016/j.apcata.2016.02.029.

[30] Nie, L., Wang, J., Tan, Q. (2017). In-situ preparation of macro/mesoporous NiO/$LaNiO_3$ pervoskite composite with enhanced methane combustion performance. *Catalysis Communications*, 97, 1-4. DOI: 10.1016/j.catcom.2017.04.010.

[31] Zhang, Y., Guo, S., Tian, Z., Zhao, Y., Hao, Y. (2019). Experimental investigation of steam reforming of methanol over La_2CuO_4/CuZnAl-oxides nanocatalysts. *Applied Energy*, 254, 113022. DOI: 10.1016/j.apenergy.2019.04.018.

[32] Bobrova, L., Bobin, A., Mezentseva, N., Sadykov, V., Thybaut, J., Marin, G. (2016). Kinetic assessment of dry reforming of methane on Pt+Ni containing composite of fluorite-like structure. *Applied Catalysis B: Environmental*, 182, 513-524. DOI: 10.1016/j.apcatb.2015.09.049.

[33] Oliveira, Â.A., Medeiros, R.L., Figueredo, G.P., Macedo, H.P., Braga, R.M., Maziviero, F.V., Melo, M.A., Melo, D.M., Vieira, M.M. (2018). One-step synthesis of $LaNiO_3$ with chitosan for dry reforming of methane. *International Journal of Hydrogen Energy*, 43, 9696-9704. DOI: 10.1016/j.ijhydene.2018.03.212.

[34] Zheng, X.-G., Tan, S.-Y., Dong, L.-C., Li, S.-B., Chen, H.-M., Wei, S.-A. (2015). Experimental and kinetic investigation of the plasma catalytic dry reforming of methane over perovskite $LaNiO_3$ nanoparticles. *Fuel Processing Technology*, 137, 250-258. DOI: 10.1016/j.fuproc.2015.02.003.

[35] Pereñíguez, R., González-DelaCruz, V.M., Holgado, J.P., Caballero, A. (2010). Synthesis and characterization of a $LaNiO_3$ perovskite as precursor for methane reforming reactions catalysts. *Applied Catalysis B: Environmental*, 93, 346-353. DOI: 10.1016/j.apcatb.2009.09.040.

[36] Chiarello, G.L., Rossetti, I., Forni, L. (2005). Flame-spray pyrolysis preparation of perovskites for methane catalytic combustion. *Journal of Catalysis*, 236, 251-261. DOI: 10.1016/j.jcat.2005.10.003.

[37] Levy, M. (2005). *Chapter 3: Perovskite Perfect Lattice.* Crystal Structure and Defect Property Predictions in Ceramic Materials, 79-114.

[38] Taran, O.P., Ayusheev, A.B., Ogorodnikova, O.L., Prosvirin, I.P., Isupova, L.A., Parmon, V.N. (2016). Perovskite-like catalysts $LaBO_3$ (B= Cu, Fe, Mn, Co, Ni) for wet peroxide oxidation of phenol. *Applied Catalysis B: Environmental*, 180, 86-93. DOI: 10.1016/j.apcatb.2015.05.055.

[39] Wu, Q., Zhao, L., Wu, M., Yao, W., Qi, M., Shi, X. (2014). Fabrication of nanofibrous A-or B-sites substituted $LaCoO_3$ perovskites with macroscopic structures and their catalytic applications. *Materials Research Bulletin*, 51, 295-301. DOI: 10.1016/j.materresbull.2013.12.038.

[40] Touahra, F., Rabahi, A., Chebout, R., Boudjemaa, A., Lerari, D., Sehailia, M., Halliche, D., Bachari, K. (2016). Enhanced catalytic behaviour of surface dispersed nickel on $LaCuO_3$ perovskite in the production of syngas: an expedient approach to carbon resistance during CO_2 reforming of methane. *International Journal of Hydrogen Energy*, 41, 2477-2486. DOI: 10.1016/j.ijhydene.2015.12.062.

[41] Qin, W., Yuan, Z., Gao, H., Zhang, R., Meng, F. (2021). Perovskite-structured $LaCoO_3$ modified ZnO gas sensor and investigation on its gas sensing mechanism by first principle. S*ensors and Actuators B: Chemical*, 341, 130015. DOI: 10.1016/j.snb.2021.130015.

[42] Yin, X., Wang, S., Wang, B., Shen, L. (2021). Chemical looping steam methane reforming using Al doped $LaMnO_{3+\delta}$ perovskites as oxygen carriers. *International Journal of Hydrogen Energy*, 46, 33375-33387. DOI: 10.1016/j.ijhydene.2021.07.192.

[43] Huang, L., Bassir, M., Kaliaguine, S. (2007). Characters of perovskite-type $LaCoO_3$ prepared by reactive grinding. *Materials Chemistry and Physics*, 101, 259-263. DOI: 10.1016/j.matchemphys.2006.08.008.

[44] Wei, T., Jia, L., Zheng, H., Chi, B., Pu, J., Li, J. (2018). $LaMnO_3$-based perovskite with in-situ exsolved Ni nanoparticles: a highly active, performance stable and coking resistant catalyst for CO_2 dry reforming of CH_4. *Applied Catalysis A: General*, 564, 199-207. DOI: 10.1016/j.apcata.2018.07.031.

[45] Liu, G., Yue, R., Jia, Y., Ni, Y., Yang, J., Liu, H., Wang, Z., Wu, X., Chen, Y. (2013). Catalytic oxidation of benzene over Ce–Mn oxides synthesized by flame spray pyrolysis. *Particuology*, 11, 454-459. DOI: 10.1016/j.partic.2012.09.013.

[46] Ghiasi, M., Delgado-Jaime, M.U., Malekzadeh, A., Wang, R.-P., Miedema, P.S., Beye, M., De Groot, F.M. (2016). Mn and Co Charge and Spin Evolutions in $LaMn_{1-x}Co_xO_3$ Nanoparticles. *The Journal of Physical Chemistry C*, 120, 8167-8174. DOI: 10.1021/acs.jpcc.6b00949.

[47] Sukumar, M., Kennedy, L.J., Vijaya, J.J., Al-Najar, B., Bououdina, M. (2018). Co^{2+} substituted $La_2CuO_4/LaCoO_3$ perovskite nanocomposites: synthesis, properties and heterogeneous catalytic performance. *New Journal of Chemistry*, 42, 18128-18142. DOI: 10.1039/C8NJ04133D.

[48] Singh, R.P., Arora, P., Nellaiappan, S., Shivakumara, C., Irusta, S., Paliwal, M., Sharma, S. (2019). Electrochemical insights into layered La_2CuO_4 perovskite: Active ionic copper for selective CO_2 electroreduction at low overpotential. *Electrochimica Acta*, 326, 134952. DOI: 10.1016/j.electacta.2019.134952.

[49] Moradi, G., Rahmanzadeh, M., Khosravian, F. (2014). The effects of partial substitution of Ni by Zn in $LaNiO_3$ perovskite catalyst for methane dry reforming. *Journal of CO_2 Utilization*, 6, 7-11. DOI: 10.1016/j.jcou.2014.02.001.

[50] Sing, K.S. (1985). Reporting physisorption data for gas/solid systems with special reference to the determination of surface area and porosity (Recommendations 1984). *Pure and applied chemistry*, 57, 603-619. DOI: 10.1351/pac198557040603.

[51] Ross, J. (1988), *Heterogenous Catalysis: Principles and Applications*, GC Bond, in: Oxford Chemistry Series, 34, Clarendon Press, Oxford (1987), p. 176, Elsevier.

[52] Jalali, R., Rezaei, M., Nematollahi, B., Baghalha, M. (2019). Preparation of $Ni/MeAl_2O_4$-$MgAl_2O_4$ (Me = Fe, Co, Ni, Cu, Zn, Mg) nanocatalysts for the syngas production via combined dry reforming and partial oxidation of methane. *Renewable Energy*, 149, 1053-1067. DOI: 10.1016/j.renene.2019.10.111.

[53] Chaisuk, C., Boonpitak, P., Panpranot, J., Mekasuwandumrong, O. (2011). Effects of Co dopants and flame conditions on the formation of Co/ZrO_2 nanoparticles by flame spray pyrolysis and their catalytic properties in CO hydrogenation. *Catalysis Communications*, 12, 917-922. DOI: 10.1016/j.catcom.2011.01.016.

[54] Shejale, A.D., Yadav, G.D. (2019). Sustainable and selective hydrogen production by steam reforming of bio-based ethylene glycol: Design and development of Ni-Cu/mixed metal oxides using M (CeO_2, La_2O_3, ZrO_2)-MgO mixed oxides. *Journal of Hydrogen Energy*, 46(6), 4808-4826. DOI: 10.1016/j.ijhydene.2019.11.031.

[55] Velasquez, M., Santamaria, A., Batiot-Dupeyrat, C. (2014). Selective conversion of glycerol to hydroxyacetone in gas phase over La_2CuO_4 catalyst. *Applied Catalysis B: Environmental*, 160, 606-613. DOI: 10.1016/j.apcatb.2014.06.006.

[56] Donphai, W., Piriyawate, N., Witoon, T., Jantaratana, P., Varabuntoonvit, V., Chareonpanich, M. (2016). Effect of magnetic field on CO_2 conversion over Cu-ZnO/ZrO_2 catalyst in hydrogenation reaction. *Journal of CO_2 Utilization*, 16, 204-211. DOI: 10.1016/j.jcou.2016.07.007.

[57] Chimentão, R., Miranda, B., Ruiz, D., Gispert-Guirado, F., Medina, F., Llorca, J., Santos, J. (2020). Catalytic performance of zinc-supported copper and nickel catalysts in the glycerol hydrogenolysis. *Journal of Energy Chemistry*, 42, 185-194. DOI: 10.1016/j.jechem.2019.07.003.

[58] Frankenburg, W.G., Komarewsky, V.I., Rideal, E.K. (1952). *Advances in catalysis*. Academic Press.

[59] Kim, D.-Y., Jeong, I.-H., Jung, S.-M. (2016). Kinetic study on carbothermic reduction of MnO_2 with graphite. *Ironmaking & Steelmaking*, 43, 526-532. DOI: 10.1080/03019233.2015.1114307.

[60] Masoom Nataj, S.M., Alavi, S.M., Mazloom, G. (2019). Catalytic performance of Ni supported on ZnO-Al_2O_3 composites with different Zn content in methane dry reforming. *Journal of Chemical Technology & Biotechnology*, 94, 1305-1314. DOI:10.1002/jctb.5887.

[61] Magalhães, R.N.S., Toniolo, F.S., Da Silva, V.T., Schmal, M. (2010). Selective CO oxidation reaction (SELOX) over cerium-doped LaCoO_3 perovskite catalysts. *Applied Catalysis A: General*, 388, 216-224. DOI: 10.1016/j.apcata.2010.08.052.

[62] Ao, M., Pham, G.H., Sage, V., Pareek, V. (2017). Selectivity enhancement for higher alcohol product in Fischer-Tropsch synthesis over nickel-substituted $La_{0.9}Sr_{0.1}CoO_3$ perovskite catalysts. *Fuel*, 206, 390-400. DOI: 10.1016/j.fuel.2017.06.036.

[63] Al-Fatesh, A.S., Fakeeha, A.H., Abasaeed, A.E. (2011). Effects of selected promoters on Ni/Y-Al_2O_3 catalyst performance in methane dry reforming. *Chinese Journal of Catalysis*, 32, 1604-1609. DOI: 10.1016/s1872-2067(10)60267-7.

[64] Pichas, C., Pomonis, P., Petrakis, D., Ladavos, A. (2010). Kinetic study of the catalytic dry reforming of CH_4 with CO_2 over $La_{2-x}Sr_xNiO_4$ perovskite-type oxides. *Applied Catalysis A: General*, 386, 116-123. DOI: 10.1016/j.apcata.2010.07.043.

[65] Kathiraser, Y., Thitsartarn, W., Sutthiumporn, K., Kawi, S. (2013). Inverse $NiAl_2O_4$ on $LaAlO_3$-Al_2O_3: unique catalytic structure for stable CO_2 reforming of methane. *The Journal of Physical Chemistry C*, 117, 8120-8130. DOI: 10.1021/jp401855x.